Pulsed Electromagnetic Excitation of a Narrow Slot Between Two Dielectric Halfspaces

Martin Štumpf, *Senior Member, IEEE*, Giulio Antonini, *Senior Member, IEEE*, and Ioan E. Lager, *Senior Member, IEEE*

***Abstract*—The transient electromagnetic (EM) excitation of a narrow slot in a perfectly electrically conducting (PEC) screen that separates two homogeneous dielectric halfspaces, a simplified model of a typical feeding structure of leaky lens antennas, is analyzed numerically in the time domain (TD). The problem is formulated using the TD reciprocity theorem of the time-convolution type and subsequently solved with the aid of the Cagniard-DeHoop method of moments (CdH-MoM). Numerical results are validated using a general-purpose EM-field solver.**

***Index Terms*—transient electromagnetic (EM) field, slot antennas, Cagniard-DeHoop method of moments (CdH-MoM), time-domain (TD) analysis.**

I. Introduction

THE need for evaluating the electromagnetic (EM) field radiation from slot antennas or undesired penetration through a crack in a shielded enclosure has prompted research into the wave diffraction by an aperture in a conducting plane (e.g. [1]–[4]). An important contribution to these efforts has been presented by Galejs [5], who thoroughly analyzed the frequency-domain (FD) response of an electric-current excited infinite slot on a lossy dielectric half-space. This model, originally intended to provide an approximate means for the performance analysis of island antennas (e.g. [6]), has been later examined with regard to leaky-wave (LW) phenomena [7], thereby providing theoretical grounds for designing slot feeding structures of ultrawideband (UWB) LW lens antennas [8]–[11].

LW antennas have a demonstrated technological effectiveness [12], [13]. At this moment, their operating principle and, as a direct consequence, their design are intrinsically related to sinusoidally in time varying EM fields, i.e. in FD. But, the increasingly sophisticated modulations currently employed for boosting the data-rate in digital transfer inherently squeeze the interval over which steady-state can be assumed. This trend justifies the attempt to understand the underlying time-domain (TD) propagation mechanism of LW antennas, with an eye on (possibly) inferring bounds for the time harmonic analysis/design. As a first step, this paper sets itself the task to go beyond the existing FD models by analyzing the slot feeding under the pulsed-field excitation in the TD. With such a goal in mind, we introduce here a novel, integral-equation (IE) computational model enabling an efficient TD analysis of the space-time distribution of magnetic-current surface density induced over a narrow finite slot in a perfectly electrically conducting (PEC) screen that separates two dielectric halfspaces.

The presented (full-wave) 3-D computational model is based on the Cagniard-DeHoop method of moments (CdH-MoM), a TD-IE technique that has recently been applied to analyzing metasurfaces [14], [15], and other basic EM radiation and scattering problems [16]–[21]. All such numerical solutions rely essentially on two basic ingredients: (a) the TD EM reciprocity theorem of the time-convolution type [22, Sec. 28.2]; (b) a version of the CdH joint-transform technique [23]. To that extent, the current work bears some similarities to the previous studies on the subject. In the computational model as proposed in this paper, however, we put forward several conceptual innovations. Indeed, papers [14], [18], [19] are limited to 2-D problem configurations only. Furthermore, the transient analysis of wire antennas [20], as well as its transmission-line approximation incorporating the effect of finite ground conductivity [17], are based on the thin-wire approximation. Therefore, the pertaining computational models do incorporate the (1-D) spatial variation of the filamentary current only, which implies a TD impedance array that is not directly applicable to the modeling of (surface) currents distributed over planar (2-D) domains. Moreover, an initial study presented in [21] is concerned with the EM plane-wave transmission through a relatively small hole in a perfectly conducting sheet, which makes it impossible to apply the pertaining (simple) model to a lumped-source excited, finite-length slot located in the plane of separation between two dielectric media – the (relatively complex) 3-D EM problem analyzed in the present paper.

First, the TD problem under consideration is formulated using the TD Lorentz reciprocity theorem [22, Sec. 28.2] (For the reader's convenience, the pertaining TD reciprocity relations are summarized in Appendix A.). In Sec. III, the starting reciprocity relation is cast into the form of complex-slowness integrals (see also Appendix A). The thus formulated problem is further solved numerically in Sec. IV. This section is supplemented with Appendix B, where it is demonstrated that (the elements of) the pertaining TD admittance array that interrelates the unknown voltage at discrete points along the narrow slot with the exciting current can be, for the piecewise-

M. Štumpf is with the Lerch Laboratory of EM Research, Dept. Radioelectronics, Faculty of Electrical Engineering and Communication, Brno University of Technology, Technická 3082/12, 616 00 Brno, The Czech Republic (e-mail: martin.stumpf@centrum.cz).

I. E. Lager is with the Terahertz Sensing Group, Faculty of Electrical Engineering, Mathematics and Computer Science, Delft University of Technology, Delft 2628 CD, The Netherlands (e-mail: i.e.lager@tudelft.nl).

G. Antonini is with the UAq EMC Laboratory, University of L'Aquila, 67 100 L'Aquila, Italy (e-mail: giulio.antonini@univaq.it).

Manuscript received May 07, 2022; revised October 21, 2022; accepted November 21, 2022. The research reported in this paper was financially supported by the Czech Science Foundation under Grant No. 20-01090S.

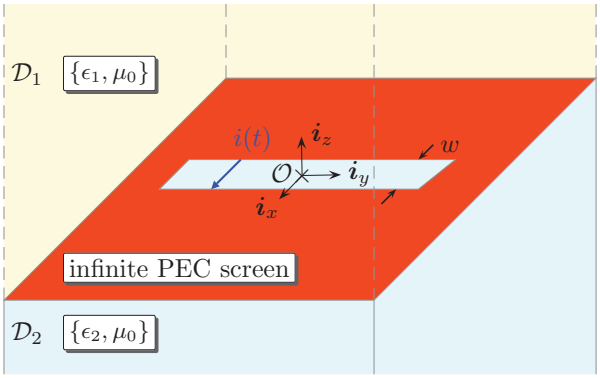

Fig. 1. A narrow slot in a PEC screen at the interface of two dielectric halfspaces.

linear space-time basis, expressed in closed form via the "Cartesian version" of the CdH technique [15, Sec. 2.1.2]. Numerical examples demonstrating the validity and efficiency of the proposed computational model are presented in Sec. V. Finally, conclusions are drawn in Sec. VI.

II. Problem Definition

The slot antenna under consideration is shown in Fig. 1. In this problem configuration, the position is specified by the coordinates $\{x, y, z\}$ with respect to a Cartesian reference frame with the origin $\mathcal{O}$ and the standard base $\{\boldsymbol{i}_x, \boldsymbol{i}_y, \boldsymbol{i}_z\}$. Consequently, the position vector can be expressed as $\boldsymbol{r} = x\boldsymbol{i}_x + y\boldsymbol{i}_y + z\boldsymbol{i}_z$. The time coordinate is denoted by t. The time-convolution operator is denoted by $*_t$. The Heaviside unit-step function is $\mathrm{H}(t)$ and the impulsive Dirac-delta distribution is represented by $\delta(t)$.

The slot in the infinite PEC screen occupies a bounded domain $\mathcal{S} = \{-w/2 \leq x \leq w/2, -L/2 \leq y \leq L/2, z = 0\}$, where $w > 0$ and $L > 0$ denote its width and length, respectively. The former dimension is supposed to be relatively small with respect to the spatial width of the excitation pulse, i.e. (EM wavespeed $\times$ excitation pulse time width). The conducting screen separates two homogeneous, isotropic and lossless half-spaces $\mathcal{D}_1$ and $\mathcal{D}_2$ that occupy $z > 0$ and $z < 0$, respectively. Their EM properties are described by (scalar, real-valued and positive) electric permittivity and magnetic permeability $\{\epsilon_1, \mu_0\}$ and $\{\epsilon_2, \mu_0\}$, respectively. The corresponding EM wave speeds and admittances are given by $c_{1,2} = (\mu_0\epsilon_{1,2})^{-1/2} > 0$ and $\eta_{1,2} = 1/\mu_0 c_{1,2} > 0$, respectively. The incorporation of losses is, in principle, feasible via the so-called Schouten-Van der Pol theorem [22, p. 1056], for instance, but at the expense of an additional integral [24].

Adopting the model introduced in Ref. [5], the excitation is incorporated via a localized discontinuity of (the y-component of) the total magnetic-field strength across the surface of slot. Assuming the uniform spatial distribution of the electric-current source in the transverse x-direction, the pertaining electric-current surface density can be described by

$$\partial J_x(x, y, t) = i(t)\Pi(x)\delta(y - y_0) \tag{1}$$

where $i(t)$ represents the exciting electric-current pulse (in A), $\Pi(x) = 1$ if $x \in [-w/2, w/2]$ and $\Pi(x) = 0$ elsewhere, and $y_0 \in (-L/2, L/2)$ denotes the position of the lumped electric-current source. In order to reduce the computational domain to the surface of slot, the scattered EM field (denoted by $^{\mathrm{s}}$) is defined here as the difference between the total fields in the presence and in the absence of the slot. Hence, associating the latter scenario with the excitation field (denoted by $^{\mathrm{e}}$), the scattered electric- and magnetic-field strengths, $\boldsymbol{E}^{\mathrm{s}}$ and $\boldsymbol{H}^{\mathrm{s}}$, respectively, can be defined as

$$\{\boldsymbol{E}^{\mathrm{s}}, \boldsymbol{H}^{\mathrm{s}}\}(\boldsymbol{r}, t) = \{\boldsymbol{E}, \boldsymbol{H}\}(\boldsymbol{r}, t) - \{\boldsymbol{E}^{\mathrm{e}}, \boldsymbol{H}^{\mathrm{e}}\}(\boldsymbol{r}, t). \tag{2}$$

This definition implies that $\boldsymbol{i}_z \times \boldsymbol{E}^{\mathrm{s}} = \boldsymbol{0}$ over the slotted PEC screen. In fact, the space-time distribution of $E_x^{\mathrm{s}}(x, y, 0, t) = E_x(x, y, 0, t)$ over the slot $\mathcal{S}$, to be associated with (the y-component of) the equivalent magnetic-current surface density $\partial K_y^{\mathrm{s}}(x, y, t) = -E_x^{\mathrm{s}}(x, y, 0, t)$, is the unknown quantity we seek.

III. Transform-Domain Representation

The presented solution strategy is based on the CdH joint-transform technique [23] that combines a one-sided time Laplace transformation with the Fourier-type slowness representation in the plane parallel to the interface. To show the notation, the s-domain expressions are given for the x-component of the electric-field strength. Accordingly, the Laplace transform is defined via

$$\hat{E}_x(x, y, z, s) = \int_{t=0}^{\infty} \exp(-st) E_x(x, y, z, t) \mathrm{d}t \tag{3}$$

for $\{s \in \mathbb{R}; s > 0\}$, and the corresponding slowness representation reads

$$\begin{aligned} \hat{E}_x(x, y, z, s) = (s/2\pi\mathrm{i})^2 \int_{\kappa=-\mathrm{i}\infty}^{\mathrm{i}\infty} \mathrm{d}\kappa \\ \times \int_{\sigma=-\mathrm{i}\infty}^{\mathrm{i}\infty} \exp[-s(\kappa x + \sigma y)] \tilde{E}_x(\kappa, \sigma, z, s) \mathrm{d}\sigma, \end{aligned} \tag{4}$$

where κ and σ are slowness parameters in the x- and y-direction, respectively. Through the use of (3) and (4) in the TD reciprocity relation (21) (see Appendix A), we may find its equivalent expressed in terms of complex-slowness integrals

$$\begin{aligned} &(s/2\pi\mathrm{i})^2 \int_{\kappa=-\mathrm{i}\infty}^{\mathrm{i}\infty} \mathrm{d}\kappa \int_{\sigma=-\mathrm{i}\infty}^{\mathrm{i}\infty} \partial \tilde{K}_y^{\mathrm{s}}(-\kappa, -\sigma, s) \\ &\qquad \times \big[\tilde{H}_y^{\mathrm{B}}(\kappa, \sigma, 0^+, s) - \tilde{H}_y^{\mathrm{B}}(\kappa, \sigma, 0^-, s)\big] \mathrm{d}\sigma \\ &= -(s/2\pi\mathrm{i})^2 \int_{\kappa=-\mathrm{i}\infty}^{\mathrm{i}\infty} \mathrm{d}\kappa \int_{\sigma=-\mathrm{i}\infty}^{\mathrm{i}\infty} \partial \tilde{J}_x(\kappa, \sigma, s) \\ &\qquad \times \partial \tilde{K}_y^{\mathrm{B}}(-\kappa, -\sigma, s) \mathrm{d}\sigma. \end{aligned} \tag{5}$$

To determine the relation between the testing source and fields, we may employ the (transform-domain) source-type EM-field representations [22, Eqs. (26.4-7) and (26.4-8)] supplied with the pertaining excitation conditions

$$\tilde{E}_x^{\mathrm{B}}(\kappa, \sigma, 0^{\pm}, s) = -\partial \tilde{K}_y^{\mathrm{B}}(\kappa, \sigma, s), \tag{6}$$

as approaching the slot from $\mathcal{D}_{1,2}$, respectively. The difference of the thus excited magnetic testing fields can then be expressed in the transform domain as

$$\tilde{H}_y^{\mathrm{B}}(\kappa,\sigma,0^+,s)-\tilde{H}_y^{\mathrm{B}}(\kappa,\sigma,0^-,s)= -\left[\eta_1\frac{c_1^2\Omega_1^2(\sigma)}{c_1\Gamma_1(\kappa,\sigma)}+\eta_2\frac{c_2^2\Omega_2^2(\sigma)}{c_2\Gamma_2(\kappa,\sigma)}\right]\partial\tilde{K}_y^{\mathrm{B}}(\kappa,\sigma,s), \quad (7)$$

where

$$\Gamma_{1,2}(\kappa,\sigma)=(1/c_{1,2}^2-\kappa^2-\sigma^2)^{1/2} \text{ with } \mathrm{Re}(\Gamma_{1,2})\geq 0 \quad (8)$$

and $\Omega_{1,2}^2(\sigma)=1/c_{1,2}^2-\sigma^2$, respectively. Since the left-hand side of (7) can be associated with the testing electric-current surface density, the expression in the brackets can be interpreted as the (transform-domain) aperture admittance. The reciprocity relation (5) with (7) is the point of departure for the numerical solution presented in the following section.

IV. Numerical Solution

The first step in the numerical solution, is the discretization of the space-time solution domain. First, the spatial discretization points along the narrow slot are chosen to be uniformly distributed along $\Delta\mathcal{S}=\{x=0, y_n=-L/2+n\Delta_y, z=0\}$ for $n=\{1,\cdots,N\}$, where N denotes the number of inner nodes and $\Delta_y=L/(N+1)$ is the spatial step. Second, in a similar fashion, the time axis is discretized as $t_k=k\Delta_t$ for $k=\{1,\cdots,M\}$, with $\Delta_t>0$ being the time step. It is noted that the uniform discretization is not mandatory and is chosen here for the sake of simplicity.

Once the solution domain is discretized, the unknown magnetic-current surface density can be expanded in terms basis functions. To that end, we use the piecewise-linear space-time expansion

$$\partial K_y^{\mathrm{s}}(x,y,t)\simeq\frac{1}{w}\sum_{n=1}^{N}\sum_{k=1}^{M}v_k^{[n]}\Pi(x)\Lambda^{[n]}(y)\Lambda_k(t), \quad (9)$$

where $v_k^{[n]}$ represents the (unknown) voltage coefficient pertaining to point (y_n,t_k), and

$$\Lambda^{[n]}(y)=\begin{cases}1+(y-y_n)/\Delta_y & \text{if } y\in[y_n-\Delta_y,y_n]\\ 1-(y-y_n)/\Delta_y & \text{if } y\in[y_n,y_n+\Delta_y].\end{cases} \quad (10)$$

In a similar manner, the temporal triangle function can be expressed via

$$\Lambda_k(t)=\begin{cases}1+(t-t_k)/\Delta_t & \text{if } t\in[t_{k-1},t_k]\\ 1-(t-t_k)/\Delta_t & \text{if } t\in[t_k,t_{k+1}].\end{cases} \quad (11)$$

Furthermore, the testing source-distribution is chosen to have the following form

$$\partial K_y^{\mathrm{B}}(x,y,t)=\delta(x)\Pi^{[q]}(y)\delta(t), \quad (12)$$

where the rectangular function, $\Pi^{[q]}(y)$, is defined for all $q=\{1,\cdots,N\}$ as $\Pi^{[q]}(y)=1$ for $y\in[y_q-\Delta_y/2, y_q+\Delta_y/2]$, while $\Pi^{[q]}(y)=0$ elsewhere.

Upon substituting the transform-domain counterparts of Eqs. (9)–(12) with (1) in the reciprocity relation (5) we end up with a system of equations in the s-domain, constituents of which can be transformed to the TD analytically with the aid of the CdH technique. Pursuing this approach, we end up with the following system of equations of the time-convolution type

$$\sum_{k=1}^{m}\big(\underline{\boldsymbol{Y}}_{m-k+1}-2\underline{\boldsymbol{Y}}_{m-k}+\underline{\boldsymbol{Y}}_{m-k-1}\big)\cdot\boldsymbol{V}_k=\boldsymbol{I}_m, \quad (13)$$

where the total TD admittance array, $\underline{\boldsymbol{Y}}$, consists of two admittance arrays, say $\underline{\boldsymbol{Y}}_{[1]}$ and $\underline{\boldsymbol{Y}}_{[2]}$, pertaining to halfspaces $\mathcal{D}_1$ and $\mathcal{D}_2$, respectively, viz

$$\underline{\boldsymbol{Y}}=\underline{\boldsymbol{Y}}_{[1]}+\underline{\boldsymbol{Y}}_{[2]} \quad (14)$$

In our notation, $\underline{\boldsymbol{Y}}_k$ represents a 2-D $[N\times N]$ admittance array at $t=t_k$, the elements of which are expressed in closed form in Appendix B. Furthermore, $\boldsymbol{V}_k$ is a 1-D $[N\times 1]$ array of unknown voltage coefficients $v_k^{[n]}$ (see Eq. (9)). Finally, the elements of the 1-D $[N\times 1]$ excitation array, $\boldsymbol{I}_m$, for the electric-current source (1) can be expressed as

$$I_m^{[q]}=-i(t_m)\big[\mathrm{H}(y_0-y_q+\Delta_y/2) -\mathrm{H}(y_0-y_q-\Delta_y/2)\big] \quad (15)$$

for all $q=\{1,\cdots,N\}$. Once both admittance and excitation arrays are fully specified, the system of equations (13) can be solved for the voltage coefficients. This can be done via the following marching-on-in-time (MOT) scheme

$$\boldsymbol{V}_m=\underline{\boldsymbol{Y}}_1^{-1}\cdot\Big[\boldsymbol{I}_m -\sum_{k=1}^{m-1}\big(\underline{\boldsymbol{Y}}_{m-k+1}-2\underline{\boldsymbol{Y}}_{m-k}+\underline{\boldsymbol{Y}}_{m-k-1}\big)\cdot\boldsymbol{V}_k\Big] \quad (16)$$

for all $m=\{1,\cdots,M\}$. Once the iterative procedure (16) is executed, the resulting voltage coefficients can be used in Eq. (9) to determine the desired magnetic-current space-time distribution over $\mathcal{S}$ and in the chosen time window of observation. Since the elements of the admittance array are derived analytically, its filling is fast and the MOT procedure is stable.

V. Illustrative Numerical Results

In this section, we shall employ the iterative solution (16) to calculate the TD voltage induced across a narrow slot of dimensions $w=1.0\,\mathrm{mm}$ and $L=50\,\mathrm{mm}$. The TD responses are observed in the time window $\{0\leq c_0t\leq 10L\}$. Throughout the examples, the lower halfspace, $\mathcal{D}_2$, is supposed to be vacuum, so that $\epsilon_2=\epsilon_0$, while the upper halfspace, $\mathcal{D}_1$, is filled by a dielectric medium with $\epsilon_1=\epsilon_{\mathrm{r}}\epsilon_0$, where $\epsilon_{\mathrm{r}}>1$ denotes its relative permittivity. Consequently, the EM wavespeeds in $\mathcal{D}_2$ and $\mathcal{D}_1$ are $c_2=c_0$ and $c_1=c_0/\sqrt{\epsilon_{\mathrm{r}}}$, respectively.

In the first example, the narrow slot on a dielectric halfspace of relative permittivity $\epsilon_{\mathrm{r}}=8.0$ is excited at the central point, $y_0=0$, by an electric-current pulse of the bipolar-triangle shape, i.e.

$$i(t)=(2i_{\mathrm{m}}/t_{\mathrm{w}})\big[t\,\mathrm{H}(t)-2\big(t-t_{\mathrm{w}}/2\big)\mathrm{H}\big(t-t_{\mathrm{w}}/2\big) +2\big(t-3t_{\mathrm{w}}/2\big)\mathrm{H}\big(t-3t_{\mathrm{w}}/2\big)-(t-2t_{\mathrm{w}})\,\mathrm{H}(t-2t_{\mathrm{w}})\big] \quad (17)$$

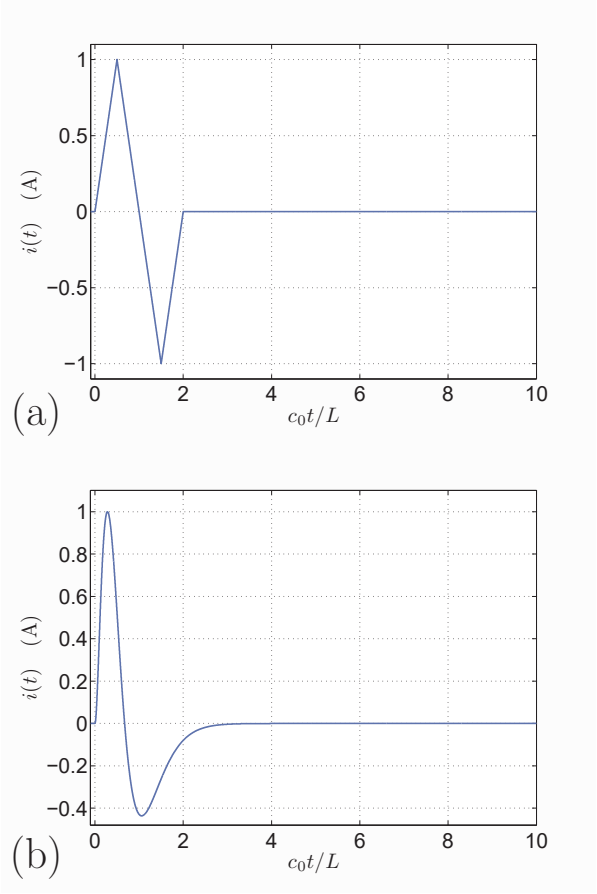

Fig. 2. Excitation electric-current pulse shapes. (a) Bipolar triangle pulse; (b) Time-differentiated power-exponential pulse.

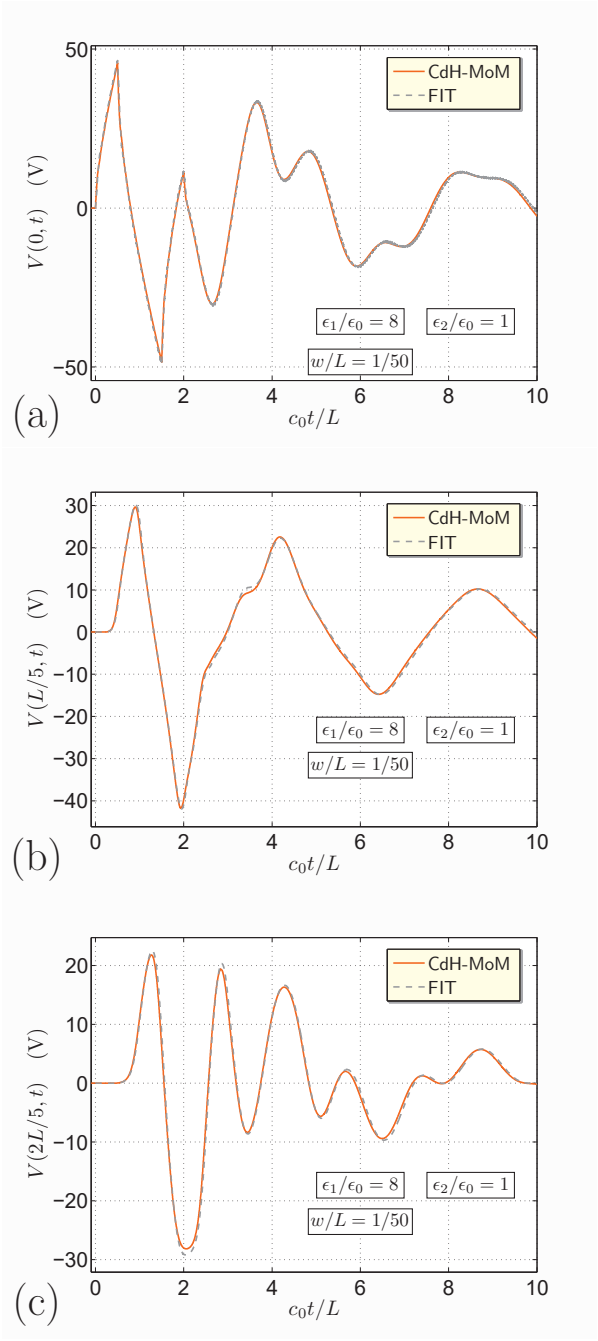

Fig. 3. Induced voltage pulse shapes due to the triangular electric-current pulse (see Fig. 2a) applied at $y_0 = 0$. Observation points are at (a) $y = 0$; (b) $y = L/5$; (c) $y = 2L/5$.

where we take the unit amplitude $i_\mathrm{m} = 1.0\,\mathrm{A}$ and $c_0 t_\mathrm{w} = L$ (see Fig. 2a). Consequently, $w/c_0 t_\mathrm{w} = 1/50$, which implies that the slot is relatively narrow. The resulting TD voltage responses as induced along the slot at $y = 0$, $y = L/5$ and $y = 2L/5$ are shown in Figs. 3a, 3b and 3c, respectively. The space-time solution domain of the CdH-MoM model was discretized in $N = 49$ spatial inner nodes, while the time step was chosen to be a tenth of slot's width, which leads to $M = 5001$ temporal points. The total computational time of a non-optimized MATLAB® code was about $200\,\mathrm{s}$, out of which approximately $25\,\%$ being spent for filling the TD admittance array and $75\,\%$ for the MOT scheme (16). For the sake of comparison, the corresponding feeding structure has also been analyzed using the finite-integration technique (FIT) as implemented in CST Studio Suite®. As can be seen in Fig. 3, the pulse shapes do correlate very well. But, owing to its volumetric mesh, the FIT model consists of about 2 millions of meshcells and the corresponding total computational time, while using 4 CPU threads, was about 30 minutes. All simulations were conducted on a standard laptop with Intel(R) Core(TM) i7-10510U CPU @ 1.80 GHz and 16 GB RAM.

In the second example, the narrow slot is activated at $y_0 = 2L/5$ by an electric-current pulse of the time-differentiated power-exponential (PE) shape [25]

$$i(t) = i_\mathrm{m} N(\nu/t_{0\mathrm{x}})(1 - t/t_{0\mathrm{x}})(t/t_{0\mathrm{x}})^{\nu-1} \times \exp[-\nu(t/t_{0\mathrm{x}} - 1)]\mathrm{H}(t) \qquad (18)$$

in which $N = (t_{0\mathrm{x}}/\nu^{1/2})[\nu^{1/2}/(\nu^{1/2} - 1)]^{\nu-1}\exp(-\nu^{1/2})$ is a normalization factor, $\nu > 1$ denotes the rising power and $t_{0\mathrm{x}}$ represents the zero-crossing time. As the latter can be associated with the pulse rise time of the corresponding unipolar PE pulse, t_w, we have $t_\mathrm{w} = t_{0\mathrm{x}}\Gamma(\nu+1)\exp(\nu)/\nu^{\nu+1}$, where $\Gamma(x)$ is the Euler gamma function. In our examples,

we take $i_{\mathrm{m}} = 1.0\,\mathrm{A}$ and $c_0 t_{\mathrm{w}} = L$, again, with $\nu = 3$. Consequently, $c_0 t_{0\mathrm{x}} \simeq 0.672L$ (see Fig. 2b).

The resulting voltage signals as calculated through both CdH-MoM and FIT models at $y = \{0, L/5, 2L/5\}$ are given in Figs. 4a–c, respectively. The agreement between the results is satisfactory, again. The computational requirements to calculate the results presented in Fig. 4 are similar to the ones indicated in the previous example, i.e. the use of CdH-MoM model reduces (a) the computational time about ten times (using the non-optimized MATLAB® code), and (b) the solution space (with accompanying memory requirements) by several orders of magnitude with respect to the general-purpose 3-D EM solver. On the other hand, standard 3-D EM solvers based on the finite-difference/element TD techniques are generally more versatile, thus enabling numerical solutions of EM problems of higher complexity.

The presented computational model can be easily generalized to incorporate multiple slots and their mutual coupling. This can be briefly demonstrated by calculating the transient voltage as induced in the second identical slot that extends along $\mathcal{R} = \{-w/2 \le x - x_0 \le w/2, -L/2 \le y \le L/2, z = 0\}$, where $|x_0| > 0$ has the meaning of the spatial offset in the x-direction with respect to the excited slot $\mathcal{S}$. Assuming the triangular-pulse excited slot from the first example, the TD voltage responses at the centre of $\mathcal{R}$ are shown in Fig. 5 for $x_0 = L/10$. To illustrate the effect of the relative permittivity, $\epsilon_{\mathrm{r}} = \epsilon_1/\epsilon_0$, the pulse shape is evaluated for $\epsilon_{\mathrm{r}} = 8$ and $\epsilon_{\mathrm{r}} = 16$. It is observed that the pulse shapes do correlate well again with the ones achieved using the FIT model. While the computational efficiency of the CdH-MoM approach is virtually independent of the halfspace permittivity, the number of meshcells of the FIT model may be exceedingly high for a high-dielectric medium.

VI. Conclusion

An efficient TD computational model for analyzing a typical feeding structure of UWB leaky lens antennas was proposed. The problem of calculating the space-time distribution of the equivalent magnetic-current surface density due to an impulsive electric-current source in the slot was approached via the CdH-MoM – a TD-IE technique based on Lorentz's reciprocity theorem and the CdH technique. It was shown that this approach leads to a time-convolution type system of equations that can be solved using a step-by-step MOT procedure. Since the elements of the pertaining TD admittance array were derived analytically in terms of elementary functions, their evaluation is computationally effortless and the MOT procedure is stable. Finally, it was demonstrated that the use of a general 3-D EM numerical tool leads to virtually equivalent results, but at the expense of significantly higher computational requirements compared to our dedicated CdH-MoM computational model. Since, in addition, the proposed TD model is easy-to-implement, it can be readily incorporated in antenna design and optimization procedures.

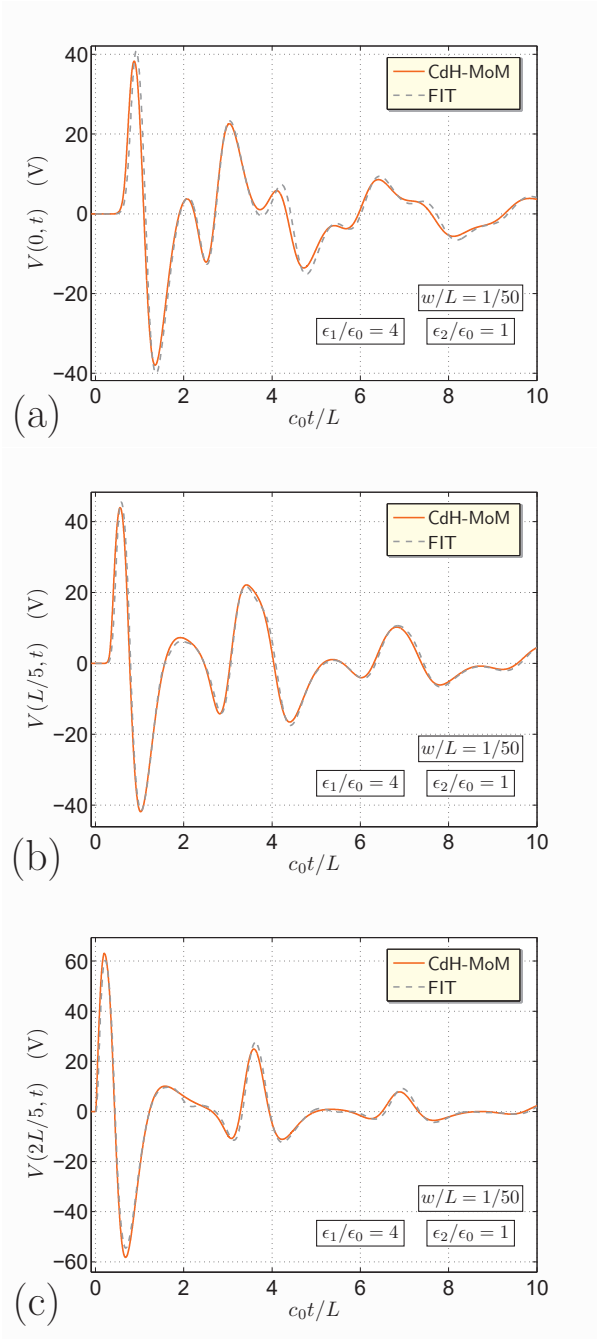

Fig. 4. Induced voltage pulse shapes due to the time-differentiated power-exponential pulse (see Fig. 2b) applied at $y_0 = 2L/5$. Observation points are at (a) $y = 0$; (b) $y = L/5$; (c) $y = 2L/5$.

Appendix A
Reciprocity Relations

The problem under consideration is formulated via the TD EM reciprocity theorem of the time-convolution type [22, Sec. 28.2]. To that end, the theorem is applied to the scattered field and to the testing field (denoted by $^{\mathrm{B}}$) that is causally related to the testing magnetic-current surface density, $\partial K_y^{\mathrm{B}}(x, y, t)$, distributed along $\mathcal{S}$. Accounting for the explicit-type boundary condition on the slotted screen as well as the causality condition at infinity [22, Sec. 28.4], the difference

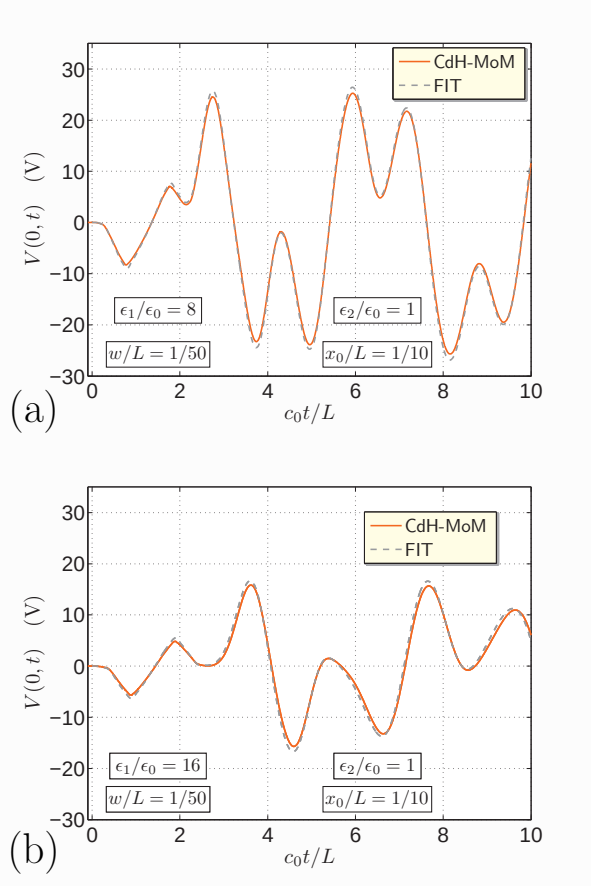

Fig. 5. Voltage pulse shapes induced in the second slot $\mathcal{R}$ due to the triangular electric-current pulse (see Fig. 2a) applied at $y_0 = 0$ of the excited slot $\mathcal{S}$. The relative permittivity of the upper halfspace is (a) $\epsilon_1/\epsilon_0 = 8$; (b) $\epsilon_1/\epsilon_0 = 16$.

of reciprocity relations pertaining to $\mathcal{D}_1$ and $\mathcal{D}_2$ leads to

$$\int_{\mathcal{S}} \partial K_y^{\mathrm{s}}(x,y,t) *_t \left[H_y^{\mathrm{B}}(x,y,0^+,t) - H_y^{\mathrm{B}}(x,y,0^-,t)\right] \mathrm{d}A = \int_{\mathcal{S}} \left[H_y^{\mathrm{s}}(x,y,0^+,t) - H_y^{\mathrm{s}}(x,y,0^-,t)\right] *_t \partial K_y^{\mathrm{B}}(x,y,t) \mathrm{d}A. \tag{19}$$

In line with Eq. (2), the scattered magnetic field on the right-hand side of Eq. (19) is further written as $H_y^{\mathrm{s}} = H_y - H_y^{\mathrm{e}}$, which yields

$$\int_{\mathcal{S}} \partial K_y^{\mathrm{s}}(x,y,t) *_t \left[H_y^{\mathrm{B}}(x,y,0^+,t) - H_y^{\mathrm{B}}(x,y,0^-,t)\right] \mathrm{d}A = \int_{\mathcal{S}} \partial J_x^{\mathrm{e}}(x,y,t) *_t \partial K_y^{\mathrm{B}}(x,y,t) \mathrm{d}A - \int_{\mathcal{S}} \partial J_x(x,y,t) *_t \partial K_y^{\mathrm{B}}(x,y,t) \mathrm{d}A, \tag{20}$$

where we expressed the jump discontinuities of the magnetic-field strength using the pertaining electric-current surface densities. As a matter of fact, $\partial J_x^{\mathrm{e}}$ can be associated with the "total surface current induced on the short-circuited aperture" [26, Sec. 9.6] that is useful, in particular, for the evaluation of EM field penetration through apertures. The second interaction integral on the right-hand side of Eq. (20) then represents the action of $\partial J_x(x,y,t)$ through which one may incorporate an electric-current source. Accounting for the latter excitation mechanism only, we take $\partial J_x^{\mathrm{e}} = 0$ and end up with

$$\int_{\mathcal{S}} \partial K_y^{\mathrm{s}}(x,y,t) *_t \left[H_y^{\mathrm{B}}(x,y,0^+,t) - H_y^{\mathrm{B}}(x,y,0^-,t)\right] \mathrm{d}A = -\int_{\mathcal{S}} \partial J_x(x,y,t) *_t \partial K_y^{\mathrm{B}}(x,y,t) \mathrm{d}A. \tag{21}$$

Recall that $\partial K_y^{\mathrm{s}}(x,y,t)$ represents the (unknown) magnetic-current surface density induced in the slot and $\partial J_x(x,y,t)$ is the excitation electric-current surface density that for the lumped electric-current source takes the form of Eq. (1). The relation between the testing source, $K_y^{\mathrm{B}}(x,y,t)$, and the limiting values of the testing fields, $H_y^{\mathrm{B}}(x,y,0^{\pm},t)$ is determined in the transform domain in Sec. III. In this respect, it is next demonstrated that the TD reciprocity relation (21) can be cast into the form of complex slowness integrals (see Eq. (5)). Considering its right-hand side, for example, application of the Laplace transform (3) allows to write

$$\int_{\mathcal{S}} \partial \hat{J}_x(x,y,s)\, \partial \hat{K}_y^{\mathrm{B}}(x,y,s) \mathrm{d}A, \tag{22}$$

where we used the standard convolution (faltung) theorem [27, 29.2.8]. In the following step, the Fourier representation (4) is used to express the electric-current surface density as

$$\partial \hat{J}_x(x,y,s) = (s/2\pi\mathrm{i})^2 \int_{\kappa=-\mathrm{i}\infty}^{\mathrm{i}\infty} \mathrm{d}\kappa \times \int_{\sigma=-\mathrm{i}\infty}^{\mathrm{i}\infty} \exp[-s(\kappa x + \sigma y)] \partial \tilde{J}_x(\kappa,\sigma,s) \mathrm{d}\sigma. \tag{23}$$

Substituting next Eq. (23) in (22) and changing the order of the integrations, we finally end up with an equivalent expression for the interaction surface integral, viz

$$\left(\frac{s}{2\pi\mathrm{i}}\right)^2 \int_{\kappa=-\mathrm{i}\infty}^{\mathrm{i}\infty} \mathrm{d}\kappa \int_{\sigma=-\mathrm{i}\infty}^{\mathrm{i}\infty} \partial \tilde{J}_x(\kappa,\sigma,s) \partial \tilde{K}_y^{\mathrm{B}}(-\kappa,-\sigma,s) \mathrm{d}\sigma. \tag{24}$$

Equation (24) is used in the main text to express the right-hand side of the reciprocity relation (5). Its left-hand side can be rewritten by following the same lines of reasoning.

Appendix B
Time-Domain Admittance Array

The elements of the TD admittance arrays as defined via Eq. (14) can be expressed as

$$Y_{[1,2]}^{[q,n]}(t) = \frac{2\eta_{1,2}}{w\Delta_y c_{1,2}\Delta_t} \big[\Phi_{1,2}(y_q - y_n + 3\Delta_y/2, t) - 3\Phi_{1,2}(y_q - y_n + \Delta_y/2, t) + 3\Phi_{1,2}(y_q - y_n - \Delta_y/2, t) - \Phi_{1,2}(y_q - y_n - 3\Delta_y/2, t)\big], \tag{25}$$

respectively, for all $q = \{1, \cdots, N\}$, $n = \{1, \cdots, N\}$ and $t > 0$, where

$$\Phi_{1,2}(y,t) = \Upsilon_{1,2}(y, w/2, t) - \Upsilon_{1,2}(y, -w/2, t) \tag{26}$$

respectively, where the TD functions $\Upsilon_{1,2}(y,x,t)$ are closely related to the generic integral function analyzed in [16,

Sec. G.1]. Indeed, it is noted that their slowness integral representations have the following form

$$\hat{\Upsilon}_{1,2}(y,x,s) = \frac{c_{1,2}^2}{8\pi^2}\int_{\sigma\in\mathbb{S}_0}\frac{\exp(s\sigma y)}{s^3\sigma^3}\Omega_{1,2}^2(\sigma)\mathrm{d}\sigma \times \int_{\kappa\in\mathbb{K}_0}\frac{\exp(s\kappa x)}{s\kappa}\frac{\mathrm{d}\kappa}{\Gamma_{1,2}(\kappa,\sigma)} \tag{27}$$

for $\{s\in\mathbb{R};s>0\}$, $\{x\in\mathbb{R};x\neq 0\}$, $\{y\in\mathbb{R};y\neq 0\}$ and the integration contours in the complex σ- and κ-planes, $\mathbb{S}_0$ and $\mathbb{K}_0$, respectively, follow the imaginary axes except for the origins, where they are indented to the right by circular arcs of vanishingly small radii (see Fig. 6). The transformation of Eq. (27) back to the TD can be performed with the help of the "Cartesian version" of the CdH technique [15, Sec. 2.1.2].

Starting with the inner integral in the complex κ-plane, the integration path, $\mathbb{K}_0$, is by virtue of Jordan's lemma and Cauchy's theorem [22, p. 1054] replaced by $\mathcal{C}\cup\mathcal{C}^*$ with $\mathcal{C}=\{\kappa(u)=-u\Omega_{1,2}(\sigma)\mathrm{sgn}(x)+\mathrm{i}0;1\le u<\infty\}$, thus representing a loop around the horizontal branch cut $\{|\Omega_{1,2}(\sigma)|\le\mathrm{Re}(\kappa)<\infty,\mathrm{Im}(\kappa)=0\}$ (see Fig. 6a). Owing to the chosen indentation, the contribution of simple pole at $\kappa=0$ must be incorporated for $x>0$. The thus transformed inner integral is subsequently substituted back in Eq. (27), where we interchange the order of the integrations with respect to σ and u. In the subsequent step, we proceed in a similar fashion in the complex σ-plane. Accordingly, the integration contour, $\mathbb{S}_0$, is first deformed into the hyperbolic CdH path, say $\mathcal{G}\cup\mathcal{G}^*$, along which $-\sigma y+u|x|\Omega_{1,2}(\sigma)=\tau$ is satisfied, where $\{r(u)/c_{1,2}\le\tau<\infty\}$ with $r(u)=(u^2x^2+y^2)^{1/2}>0$ represents the real-valued and positive (time) parameter (see Fig. 6b). In addition, the contribution of the pole at $\sigma=0$ is for $y>0$ accounted for. Once we then change the variable of integration from σ to τ, we arrive at a double integral with respect to u and τ. In this result, we further change the order of the integrations and end up with the integral expression whose form resembles the one of Laplace-transform integral (3). Since the Laplace-transform parameter, s, is kept real-valued and positive throughout the analysis, Lerch's uniqueness theorem [28, Appendix] ensures the existence of the unique TD original function. The latter can be finally expressed as follows [16, cf. Eqs. (G.24), (G.25) and (G.30)]

$$\begin{aligned}\Upsilon_{1,2}(y,x,t) &= \frac{\mathrm{sgn}(x)\mathrm{sgn}(y)}{12\pi}\int_{\xi=r}^{c_{1,2}t}(c_{1,2}t-\xi)^3\psi(y,x,\xi)\mathrm{d}\xi\\ &+\frac{\mathrm{sgn}(x)\mathrm{H}(y)}{4\pi}\Bigg\{|x|\left(c_{1,2}^2t^2-y^2+\frac{x^2}{3}\right)\cosh^{-1}\left(\frac{c_{1,2}t}{|x|}\right)\\ &-\alpha\tan^{-1}\left(\beta_x\right)-7c_{1,2}tx^2\beta_x/6\Bigg\}\mathrm{H}(c_{1,2}t-|x|)\\ &+\frac{\mathrm{sgn}(y)\mathrm{H}(x)}{4\pi}\Bigg\{|y|\left(c_{1,2}^2t^2-\frac{y^2}{6}\right)\cosh^{-1}\left(\frac{c_{1,2}t}{|y|}\right)\\ &-\alpha\tan^{-1}\left(\beta_y\right)-5c_{1,2}ty^2\beta_y/3\Bigg\}\mathrm{H}(c_{1,2}t-|y|)\\ &+\alpha\mathrm{H}(x)\mathrm{H}(y)\mathrm{H}(t)/4,\end{aligned} \tag{28}$$

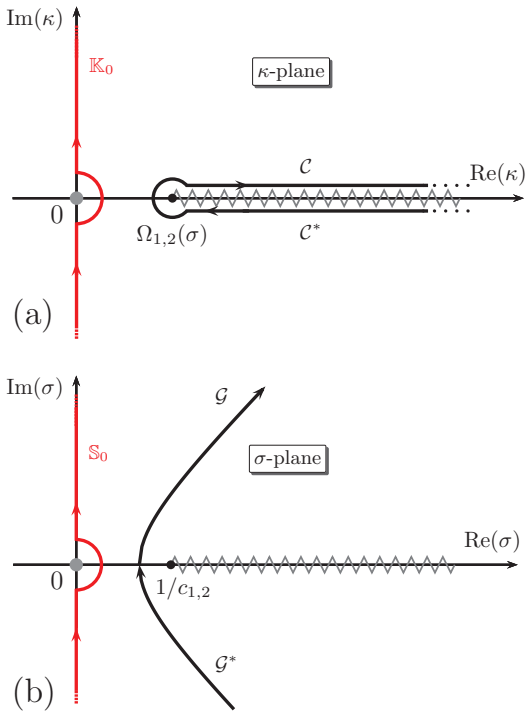

Fig. 6. Complex planes with their integration paths. (a)κ-plane with the CdH path $\mathcal{C}\cup\mathcal{C}^*$ for $x<0$; (b) σ-plane with the CdH path $\mathcal{G}\cup\mathcal{G}^*$ for $y<0$.

respectively, where $r=(x^2+y^2)^{1/2}>0$, and

$$\alpha = c_{1,2}t\left(c_{1,2}^2t^2/6-y^2\right) \tag{29}$$

$$\beta_\varsigma = \left(c_{1,2}^2t^2/\varsigma^2-1\right)^{1/2}\text{ for }\varsigma=\{x,y\}. \tag{30}$$

Furthermore, we used

$$\begin{aligned}\psi(y,x,\xi) &= \left(1/\xi_x+1/\xi_y\right)/2\xi\\ &-\frac{1}{16}\frac{x^4}{y^2\xi^3}\frac{1}{\xi_x^5}\Bigg[3\frac{\xi^8}{x^8}+6\frac{\xi^6}{x^6}\left(\frac{y^2}{x^2}-1\right)\\ &+\frac{\xi^4}{x^4}\left(15\frac{y^4}{x^4}-10\frac{y^2}{x^2}+3\right)+4\frac{\xi^2}{x^2}\frac{y^2}{x^2}\left(1-5\frac{y^2}{x^2}\right)\\ &+8\frac{y^4}{x^4}\Bigg]-\frac{1}{2}\frac{y^2}{\xi^3}\frac{1}{\xi_y}-\frac{3}{16}\frac{\xi}{y^2}\frac{1}{\xi_x^5}\Bigg[3\frac{\xi^4}{x^4}+2\frac{\xi^2}{x^2}\left(\frac{y^2}{x^2}-3\right)\\ &+\frac{y^2}{x^2}\left(3\frac{y^2}{x^2}-2\right)+3\Bigg]+\frac{3}{4}\frac{\xi}{y^2}\frac{1}{\xi_x^3}\left(\frac{\xi^2}{x^2}+\frac{y^2}{x^2}-1\right).\end{aligned} \tag{31}$$

with

$$\xi_\varsigma = \left(\xi^2/\varsigma^2-1\right)^{1/2}\text{ for }\varsigma=\{x,y\}. \tag{32}$$

As the closed-form expression (28) can be easily implemented in any computing platform such as MATLAB®, the evaluation of the TD admittance arrays through (25) and (26) is computationally (almost) effortless. The most expensive task in this respect could be the time-convolution integral in Eq. (28). As its integrand does not exhibit any nonintegrable singularities, it can be readily carried out via a standard Gaussian quadrature or using the recursive convolution technique [15, Appendix L]. Yet more efficient approach is to handle the integration

analytically via a multiple application of integration by parts. Following this strategy, we may write

$$\int_{\xi=r}^{ct}(ct-\xi)^3\psi(y,x,\xi)\mathrm{d}\xi = -(ct-r)^3\partial_\xi^{-1}\psi(y,x,r) - 3(ct-r)^2\partial_\xi^{-2}\psi(y,x,r) - 6\,(ct-r)\partial_\xi^{-3}\psi(y,x,r) - 6\,\partial_\xi^{-4}\psi(y,x,r) + 6\,\partial_\xi^{-4}\psi(y,x,ct), \quad (33)$$

where ∂_ξ^{-n} denotes the nth integration with respect to ξ. Since $\psi(y,x,\xi)$ is available in closed form via (31), the integrals on the right-hand side of Eq. (33) are attainable analytically. Consequently, the elements of the TD admittance array can be expressed solely in terms of elementary functions, which enables its fast evaluation.

ACKNOWLEDGMENT

This paper is dedicated to Lorentz Chair Emeritus Professor Adrianus T. de Hoop of TU Delft on the occasion of his 95th birthday. His truly pioneering research achievements, the "Cagniard-DeHoop technique" and the wavefield reciprocity approach, paved the way for the development of the Cagniard-DeHoop method of moments, and stimulated many of his students and colleagues to embark on the exciting quest for beauty of science.

The research reported in this paper was carried out during a research stay M. Štumpf had effectuated at the TeraHertz Sensing Group, TU Delft. The stay was financed by the Czech Ministry of Education, Youth and Sports through Project No. CZ.02.2.69/0.0/0.0/18_053/0016962.

REFERENCES

[1] H. Levine and J. Schwinger, "On the theory of diffraction by an aperture in an infinite plane screen. I," *Phys. Rev.*, vol. 74, no. 8, pp. 958–974, 1948.

[2] C. J. Bouwkamp, "Diffraction theory," *Rep. Prog. Phys.*, vol. 17, pp. 35–100, 1953.

[3] F. de Meulenaere and J. G. Van Bladel, "Polarizability of some small apertures," *IEEE Trans. Antennas Propag.*, vol. 25, no. 2, pp. 198–205, 1977.

[4] C. M. Butler, Y. Rahmat-Samii, and R. Mittra, "Electromagnetic penetration through apertures in conducting surfaces," *IEEE Trans. Antennas Propag.*, vol. 26, no. 1, pp. 82–93, 1978.

[5] J. Galejs, "Excitation of slots in a conducting screen above a lossy dielectric half space," *IRE Trans. Antennas Propag.*, vol. 10, no. 4, pp. 436–443, 1962.

[6] M. Morgan, "An island as a natural very-low-frequency transmitting antenna," *IRE Trans. Antennas Propag.*, vol. 8, no. 5, pp. 528–530, 1960.

[7] A. Neto and S. Maci, "Green's function for an infinite slot printed between two homogeneous dielectrics – part I: Magnetic currents," *IEEE Trans. Antennas Propag.*, vol. 51, no. 7, pp. 1572–1581, 2003.

[8] A. Neto, S. Bruni, G. Gerini, and M. Sabbadini, "The leaky lens: A broad-band fixed-beam leaky-wave antenna," *IEEE Trans. Antennas Propag.*, vol. 53, no. 10, pp. 3240–3246, 2005.

[9] S. Bruni, A. Neto, and F. Marliani, "The ultrawideband leaky lens antenna," *IEEE Trans. Antennas Propag.*, vol. 55, no. 10, pp. 2642–2653, 2007.

[10] A. Neto, "UWB, non dispersive radiation from the planarly fed leaky lens antenna—part 1: Theory and design," *IEEE Trans. Antennas Propag.*, vol. 58, no. 7, pp. 2238–2247, 2010.

[11] M. A. Campo, D. Blanco, S. Bruni, A. Neto, and N. Llombart, "On the use of fly's eye lenses with leaky-wave feeds for wideband communications," *IEEE Trans. Antennas Propag.*, vol. 68, no. 4, pp. 2480–2493, 2020.

[12] N. Llombart, G. Chattopadhyay, A. Skalare, and I. Mehdi, "Novel terahertz antenna based on a silicon lens fed by a leaky wave enhanced waveguide," *IEEE Trans. Antennas Propag.*, vol. 59, no. 6, pp. 2160–2168, 2011.

[13] N. Llombart and A. Neto, "THz time-domain sensing: The antenna dispersion problem and a possible solution," *IEEE Trans. Terahertz Sci. Tech.*, vol. 2, no. 4, pp. 416–423, 2012.

[14] M. Štumpf, "Pulsed electromagnetic scattering by metasurfaces – a numerical solution based on the Cagniard-DeHoop method of moments," *IEEE Trans. Antennas Propag.*, vol. 69, no. 11, pp. 7761–7770, 2021.

[15] ——, *Metasurface Electromagnetics: The Cagniard-DeHoop Time-Domain Approach*. London, UK: IET, 2022.

[16] ——, *Time-Domain Electromagnetic Reciprocity in Antenna Modeling*. Hoboken, NJ: IEEE Press–Wiley, 2019.

[17] ——, "Transient response of a transmission line above a thin conducting sheet – a numerical model based on the Cagniard-DeHoop method of moments," *IEEE Antennas Wireless Propag. Lett.*, vol. 20, no. 9, pp. 1829–1833, 2021.

[18] M. Štumpf, "Time-domain electromagnetic scattering by a two-dimensional narrow groove – a solution based on the Cagniard-DeHoop method of moments," *IEEE Antennas Wireless Propag. Lett.*, vol. 21, no. 3, pp. 586–589, 2021.

[19] M. Štumpf, I. E. Lager, G. Antonini, and G. A. E. Vandenbosch, "Pulsed em field scattering from a narrow superconducting strip: A solution based on the marching-on-in-time Cagniard-DeHoop method," in *Proc. 15th European Conf. Antennas Propag.*, Dusseldorf, Germany, April 2021, pp. 1–3.

[20] M. Štumpf, I. E. Lager, and G. Antonini, "Time-domain analysis of thin-wire structures based on the Cagniard-DeHoop method of moments," *IEEE Trans. Antennas Propag.*, vol. 70, no. 6, pp. 4655–4662, 2022.

[21] M. Štumpf, "Pulsed electromagnetic field transmission through a small rectangular aperture: a solution based on the Cagniard–DeHoop method of moments," *Algorithms*, vol. 15, no. 6, pp. 4655–4662, 2022.

[22] A. T. de Hoop, *Handbook of Radiation and Scattering of Waves*. London, UK: Academic Press, 1995.

[23] ——, "A modification of Cagniard's method for solving seismic pulse problems," *Appl. Sci. Res.*, vol. B, no. 8, pp. 349–356, 1960.

[24] F. M. Tesche, "On the inclusion of loss in time-domain solutions of electromagnetic interaction problems," *IEEE Trans. Electromagn. Compat.*, vol. 32, no. 1, pp. 1–4, 1990.

[25] I. E. Lager, A. T. de Hoop, and T. Kikkawa, "Model pulses for performance prediction of digital microelectronic systems," *IEEE Trans. Compon. Packag. Manuf. Technol.*, vol. 2, no. 11, pp. 1859–1870, 2012.

[26] J. G. van Bladel, *Electromagnetic Fields*, 2nd ed. Hoboken, NJ: John Wiley & Sons, 2007.

[27] M. Abramowitz and I. A. Stegun, *Handbook of Mathematical Functions*. New York, NY: Dover Publications, 1972.

[28] M. Štumpf, *Electromagnetic Reciprocity in Antenna Theory*. Hoboken, NJ: IEEE Press–Wiley, 2018.

Martin Štumpf (M'15 - SM'20) received his Ph.D. degree in electrical engineering from the Brno University of Technology (BUT), Brno, The Czech Republic, in 2011. After his Ph.D. research, he spent a year and a half as a Post-Doctoral Fellow with KU Leuven, Belgium. He is currently an Associate Professor of Theoretical Electrical Engineering with the Lerch Laboratory of EM Research, BUT. During a three-month period in 2018, he was a Visiting Professor at the UAq EMC Laboratory, University of L'Aquila, Italy. He has authored the books "*Electromagnetic Reciprocity in Antenna Theory*" (Wiley–IEEE Press, 2017), "*Pulsed EM Field Computation in Planar Circuits: The Contour Integral Method*" (CRC Press, 2018), "*Time-Domain Electromagnetic Reciprocity in Antenna Modeling*" (Wiley–IEEE Press, 2019), and "*Metasurface Electromagnetics: The Cagniard-DeHoop Time-Domain Approach*" (IET, 2022). His main research interests include modeling of electromagnetic wave phenomena with an emphasis on antenna theory and EMC.

Giulio Antonini (M'94 - SM'05) received the Laurea degree (*cum laude*) in electrical engineering from the University of L'Aquila, L'Aquila, Italy, in 1994 and the Ph.D. degree in electrical engineering from University of Rome "La Sapienza" in 1998. Since 1998, he has been with the UAq EMC Laboratory, University of L'Aquila, where he is currently a Professor. He has coauthored the book "*Circuit Oriented Electromagnetic Modeling Using the PEEC Techniques*", (Wiley–IEEE Press, 2017). His scientific interests are in the field of computational electromagnetics.

Ioan E. Lager (SM'14) received PhD degrees in Electrical Engineering from Delft University of Technology, the Netherlands (1996), and from Transilvania University of Braşov, Romania. He successively occupied research and academic positions with Transilvania University of Braşov and Delft University of Technology, where he is currently an Associate Professor. In 1997 he was a Visiting Scientist with Schlumberger-Doll Research, Ridgefield, CT, USA. Dr. Lager endeavors towards bridging the gap between electromagnetic field theory and the design, implementation and measurement of antenna front-end architectures. His interests are in applied electromagnetics, especially time-domain propagation and applications, and antenna engineering, with an emphasis on nonperiodic (interleaved) array antenna architectures.